Ultrastructural Characterization of Peptide-Induced Membrane Fusion and Peptide Self-Assembly in the Lipid Bilayer

Anne S. Ulrich,* Willem Tichelaar,# Günter Förster,§ Olaf Zschörnig,¶ Sevil Weinkauf,# and Helmut W. Meyer#
*Institut für Molekularbiologie, Friedrich-Schiller-Universität Jena, 07745 Jena; #Institut für Ultrastrukturforschung des Klinikums der Friedrich-Schiller-Universität Jena, 07743 Jena; §Institut für Physikalische Chemie, Martin-Luther-Universität Halle, 06108 Halle; and ¶Institut für Medizinische Physik und Biophysik, 04103 Leipzig

ABSTRACT The peptide sequence B18, derived from the membrane-associated sea urchin sperm protein bindin, triggers fusion between lipid vesicles. It exhibits many similarities to viral fusion peptides and may have a corresponding function in fertilization. The lipid-peptide and peptide-peptide interactions of B18 are investigated here at the ultrastructural level by electron microscopy and x-ray diffraction. The histidine-rich peptide is shown to self-associate into two distinctly different supramolecular structures, depending on the presence of Zn^{2+}, which controls its fusogenic activity. In aqueous buffer the peptide per se assembles into β-sheet amyloid fibrils, whereas in the presence of Zn^{2+} it forms smooth globular clusters. When B18 per se is added to uncharged large unilamellar vesicles, they become visibly disrupted by the fibrils, but no genuine fusion is observed. Only in the presence of Zn^{2+} does the peptide induce extensive fusion of vesicles, which is evident from their dramatic increase in size. Besides these morphological changes, we observed distinct fibrillar and particulate structures in the bilayer, which are attributed to B18 in either of its two self-assembled forms. We conclude that membrane fusion involves an α-helical peptide conformation, which can oligomerize further in the membrane. The role of Zn^{2+} is to promote this local helical structure in B18 and to prevent its inactivation as β-sheet fibrils.

INTRODUCTION

Many amphiphilic peptides have a high affinity for lipid bilayers, but only certain sequences are able to induce membrane fusion (Shai, 1995; Brasseur et al., 1997; Durell et al., 1997). An investigation of their distinct binding modes will help to clarify their mechanism of action and may lead to a better understanding of the fusogenic functions of larger proteins (Hughson, 1995; Hernandez et al., 1996; Monck and Fernandez, 1996). Much of the current knowledge of lipid-peptide interactions during membrane fusion is based on fluorescence studies of peptide binding, lipid mixing, contents leakage, and vesicle aggregation (Ohki et al., 1998). Conformational changes of a peptide, when it binds to a membrane, are readily characterized by circular dichroism (CD) or vibrational spectroscopy. Beyond the local interactions at a molecular level, however, there is comparatively little information available about fusion-competent systems on a mesoscopic scale. With this in mind, electron microscopy (EM) and x-ray diffraction can be used to monitor an increase in vesicle size, to examine the effects of a peptide on bilayer morphology and surface texture, and to detect nonbilayer phases (Verkleij et al., 1984; Colotto and Epand, 1997; Burger, 1998). Another significant question, also to be addressed here by ultrastructural means, concerns the aggregation behavior and higher oligomeric states of fusogenic peptides.

The most thoroughly characterized fusogenic peptides are derived from enveloped viruses, and there have been a few reports on similar sequences that appear to be involved in fertilization (Durell et al., 1997; Pécheur et al., 1999). Most of these peptides are rather hydrophobic and prone to self-association. A low solubility in aqueous buffer or oligomerization in the membrane-bound state is implicit from previous studies on the fusion peptides of HIV gp41 (Rafalski et al., 1990; Gordon et al., 1992; Martin et al., 1993; Slepushkin et al., 1993; Nieva et al., 1994; Pereira et al., 1997; Kliger et al., 1997), influenza hemagglutinin (Wharton et al., 1988; Rafalski et al., 1991; Gray et al., 1996), Sendai virus (Rapaport and Shai, 1994), feline leukemia virus (Davies et al., 1998a,b), measles virus (Epand et al., 1992), and the putative sperm fusion protein PH-30 (Muga et al., 1994; Niidome et al., 1997). Interestingly, the biologically active state of fusogenic peptides and proteins appears to involve higher oligomeric forms, according to studies with model membranes as well as biological systems (Rapaport and Shai, 1994; Shai, 1995; Gray et al., 1996; Monck and Fernandez, 1996; Kliger et al., 1997).

Membrane-associated peptides often show a remarkably polymorphic structural behavior, and experimental conditions can strongly affect their conformation and activity (Davies et al., 1998a,b). Many fusion peptides require an α-helical conformation to be functional (Takahashi, 1990; Gordon et al., 1992; Martin et al., 1993; Rapaport and Shai, 1994; Kliger et al., 1997; Ulrich et al., 1998, Glaser et al., 1999), but in other cases a β-sheet has been proposed as the active structure (Nieva et al., 1994; Muga et al., 1994; Pereira et al., 1997; Niidome et al., 1997). Peptides with a

Received for publication 6 July 1998 and in final form 1 April 1999.

Address reprint requests to Dr. Anne S. Ulrich, Institut für Molekularbiologie, Friedrich-Schiller-Universität Jena, Winzerlaer Strasse 10, 07745 Jena, Germany. Tel.: +49-3641-6575-72; Fax: +49-3641-6575-20; E-mail: ulrich@molebio.uni-jena.de.

Dr. Tichlaar's present address is Max-Planck-Institut für Medizinische Forschung, 69120 Heidelberg, Germany.

0006-3495/99/08/829/13 $2.00

β-sheet structure are often found to be extensively self-associated. Certain viral fusion peptides have indeed been reported to form amyloid-like fibrils both in aqueous buffer and in the membrane-bound state (Brasseur et al., 1997). In view of this distinctive fibrillar appearance, it is not unreasonable to ask whether the Alzheimer Aβ and other amyloidogenic peptides follow a similar self-assembly mechanism, leading to a perturbation of cellular membranes. The medical relevance of such neurotoxic peptides systems calls for intense research into the lipid interactions of fibrillar peptides (Li et al., 1995; McLaurin et al., 1996; Pillot et al., 1996; Terzi et al., 1997; Kawahara et al., 1997; Forloni et al., 1996; McLaurin et al., 1998).

Here we investigate the fusogenic peptide B18, which is a distinct amphiphilic sequence of the sea urchin protein bindin. This acrosomal protein plays a key role in fertilization by mediating the adhesion and fusion between sperm and egg (Hofmann and Glabe, 1994; Vacquier et al., 1995). Parts of the protein are highly divergent and are responsible for species-specific recognition, but the sequence around B18 is fully conserved. Previous studies have shown that synthetic peptides from this region inhibit fertilization (DeAngelis and Glabe, 1990a; Minor et al., 1993). Specifically the B18 peptide can imitate several functions of the much larger parent protein (Ulrich at al., 1998), which include the binding, aggregation, and fusion of neutral lipid vesicles (Glabe, 1985a,b; Miraglia and Glabe, 1993; Miraglia, 1993; Loidl-Stahlhofen et al., 1996), as well as the binding to sulfated polysaccharides from the egg surface (DeAngelis and Glabe, 1990b). These activities of B18 are promoted only in the presence of Zn^{2+}. This particular ion is also contained in the parent protein in a stoichiometric amount, where it is bound via the histidine-rich motif within the B18 sequence (DeAngelis and Glabe, 1990b). It has recently been suggested that B18 becomes fusogenic by forming an oligomeric complex with Zn^{2+} via its histidine side chains, whereby the peptide assumes a partially α-helical conformation (Ulrich et al., 1998; Glaser et al., 1999). Overall, B18 shares many characteristics with viral fusion peptides (Durell et al., 1997), although we note that the parent protein bindin is peripherally associated with the membrane, unlike any viral fusion protein with a transmembrane anchor (Hernandez et al., 1996).

Functionally, the most convenient aspect of the B18 model system lies in our ability to switch the fusogenic activity of the peptide on or off, simply by the addition of Zn^{2+} (Ulrich at al., 1998). Under both active and inactivated conditions, we have used electron microscopy and x-ray diffraction to characterize not only the morphology of the lipid bilayer, but also the appearance of the peptide when it is incubated in the presence and absence of vesicles. We have observed different kinds of self-assembled peptidic structures, both in aqueous buffer and in the membrane. Rather than aggregating as an amorphous lump, B18 forms either smooth globular particles or fibrillar structures, depending on its functional state. Based on these observations, it is possible to interpret the ultrastructural features of the system in terms of the conformational behavior of the peptide.

MATERIALS AND METHODS

Lipids

Bovine brain sphingomyelin (SM), cholesterol (Chol), 1,2-dimyristoyl-*sn*-glycero-3-phosphocholine (DMPC), 1,2-dimyristoyl-*sn*-glycero-3-phospho-*rac*-(1-glycerol) (DMPG), 1,2-dioleoyl-*sn*-glycero-3-phosphoethanolamine (DOPE), and egg yolk L-α-lecithin (egg-PC) were purchased from Avanti Polar Lipids (Alabaster, AL). Liposomes were prepared by codissolving the lipid in chloroform (plus methanol, if required) and drying under N_2. The mixture was resuspended by vortexing in buffer (10 mM HEPES, 100 mM NaCl, pH 7.4) at a final lipid concentration of ~10 mg/ml, followed by 10 freeze-thaw cycles using 50°C warm water. A uniform population of large unilamellar vesicles (LUVs) was obtained by repeated high-pressure extrusion (Lipex extruder from Biomembranes, Vancouver, BC) of the suspension through a polycarbonate Unipore membrane (100 nm pore size; Millipore), at a temperature above the gel-to-fluid phase transition of the lipid.

Peptide synthesis

The peptide B18 (LGLLLRHLRHHSNLLANI) was synthesized semiautomatically, using solid-phase resin and Fmoc protecting groups. The crude peptide was purified by reverse-phase high-performance liquid chromatography on a water/acetonitrile gradient with 0.1% trifluoroacetic acid. The purity and mass of the product (M_W = 2090 g/mol) were checked by electrospray mass spectrometry, and the amount of lyophilized peptide was determined gravimetrically. Stock solutions were prepared by dissolving the peptide at 10 mM in double distilled water, giving pH ~4, where it is fully soluble.

Negative stain electron microscopy

To induce self-association of B18 in different aggregation states, the peptide was added from the acidic stock solution to buffer at pH 7.5 (100 mM Tris) to give a 1 mM final peptide concentration. Different salt conditions were tested with 50 or 200 mM NaCl, and with 2 mM or 50 mM EDTA. In another set of samples, 1 mM or 5 mM $ZnCl_2$ was added to form metallocomplexes with the peptide. Control experiments were carried out with buffers and stock solutions alone and at pH 4.0 (100 mM acetate). Negatively stained specimens were prepared for electron microscopy (EM) according to the two-step droplet method, with 2% uranyl acetate as a stain. Carbon-coated grids were used, which had been glow-discharged in residual air for ~15 s. The specimens were examined in a Philips CM120 electron microscope, and the magnification was calibrated using a cross-grating with 2160 lines/mm.

Freeze-fracture electron microscopy

To monitor membrane fusion by EM, the experimental conditions were adopted from previous fluorescence and light scattering assays (Ulrich et al., 1998), but higher concentrations have been used here to increase the density of material. The peptide from the stock solution was mixed with 200 μl of the liposome suspension (10 mg/ml), to give a final peptide concentration of 500 μM in 10 mM HEPES (100 mM NaCl, pH 7.4). This corresponds to a lipid/peptide ratio of 30:1 (mol/mol), unless stated otherwise. In another set of samples, $ZnCl_2$ was also present in a total concentration of 0.6, 1.6, or 3.3 mM. All samples were prepared at room temperature and stored at 4°C in the refrigerator. For EM, the samples were incubated at the desired temperature in a water bath (20°C, 30°C, or 45°C) for at least half an hour, and all instruments for handling the material were also equilibrated at the required temperature. The lipid-peptide suspensions

were sandwiched between small copper plates, which were then thermally quenched by plunging them into liquid propane. The frozen samples were fractured in a BAF400 freeze-etching unit (BAL-TEC, Balzers Liechtenstein) at −150°C and shadowed with Pt/C. Some of the samples were subjected to an etching period of 30 s at −100°C upon fracturing. The carbon-coated replicas were cleaned with chloroform and examined under a CEM 902A (Zeiss, Germany) electron microscope.

X-ray diffraction

For x-ray analysis the lipid and peptide were reconstituted with one another by cosolubilization, to obtain homogeneous samples with a high lipid/peptide ratio of 10:1. A total of 3 mg lipid (either SM plus Chol (80/20), or DMPC) was dissolved together with 1 mg B18 in trifluoroethanol (TFE) and dried under N_2 and then under high vacuum overnight. Samples were hydrated with a threefold excess (w/w) of 200 mM HEPES buffer at pH 7.5. Pure B18 fibrils were prepared by adding 10 μl buffer directly to 1 mg of the lyophilized peptide. Control samples consisted of the lipids alone, hydrated with either buffer or distilled H_2O. For x-ray diffraction, the samples were sealed in thin-wall capillary tubes, which were rotated during the measurements to improve signal averaging. A transmission x-ray powder diffraction system (STOE and CIE, Darmstadt, Germany) was used, operating with CuKα_1 radiation (Ge(111) monochromator) and a stationary curved position-senstitive detector ($0° < 2\theta < 40°$). A high-temperature attachment was used to control the range between −40°C and 50°C in a N_2 stream to a precision within ±0.2 K. Diffractograms were corrected for parasitic scattering in the background. Data were processed with Origin (Microcal) and deconvoluted after a fit procedure with sufficiently good statistics (correlation coefficient > 0.985). From the long spacings the bilayer repeat distances of the multilamellar liposomes were calculated. The short spacings, which characterize the lateral packing of the chains, are compared here only qualitatively with respect to their position, intensity, and broadening.

RESULTS AND DISCUSSION

Self-assembly of B18 in buffer, as monitored by negative stain EM

The B18 peptide (LGLLLRHLRHHSNLLANI) is fully water-soluble only at acidic pH, where it carries a net charge of +5. At pH > 7, the three histidine side chains become deprotonated, and B18 tends to self-aggregate in a concentration-dependent manner. Negative stain electron microscopy of the dispersion reveals long fibrillar structures (Fig. 1 *A*), which are closely reminiscent of amyloid. The ribbons typically consist of three to five protofilaments with widths of ~5 nm each. Most ribbons are twisted with a pitch of ~100 nm, whereas a few are unwound or even appear to be assembled into straight tubular rods. The presence of NaCl promotes the formation of wider ribbons and more elaborate structures, suggesting that the charges on the protofilaments (i.e., two arginine residues on B18) are better shielded at high ionic strength. Self-assembly is prevented by EDTA, in good agreement with earlier observations that this anion forms a complex with the peptide via its arginine side chains (Ulrich at al., 1998).

Fibrillar precipitates from various unrelated proteins are generally called "amyloid" when they stain with Congo Red. The B18 fibrils stained positively and showed the expected green birefringence under crossed polarizers, which is taken as evidence of their genuine amyloid nature.

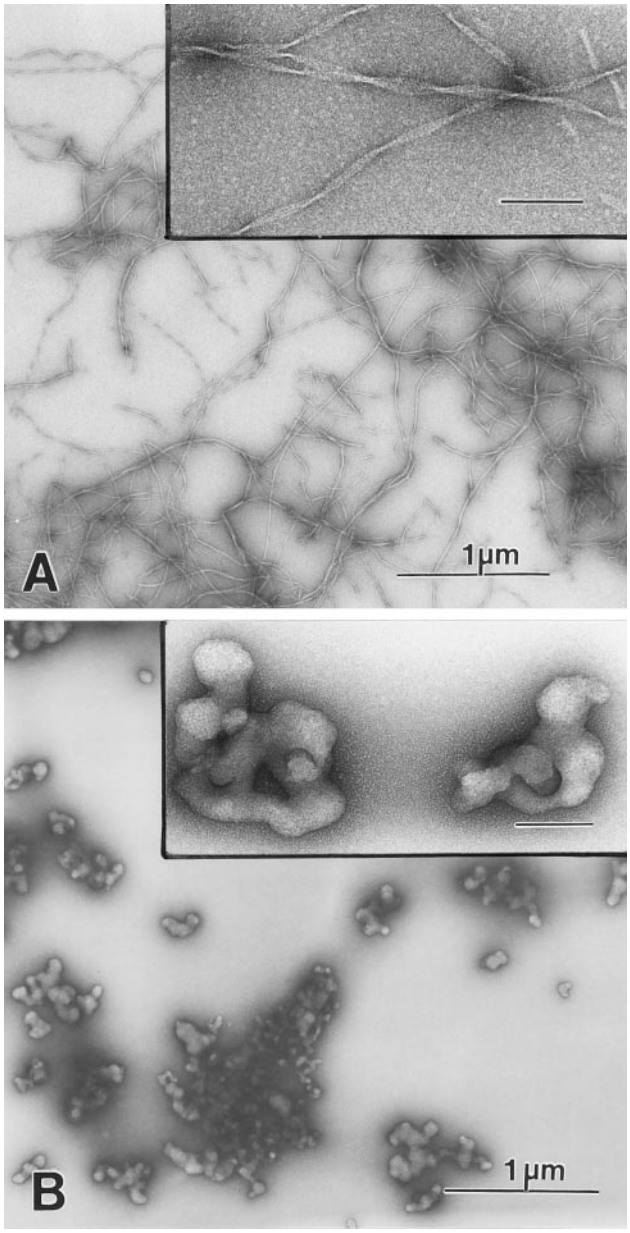

FIGURE 1 Self-assembly of the B18 peptide in aqueous buffer at pH 7.5, as observed by negative stain EM. (*A*) The peptide per se forms characteristic amyloid fibrils, consisting of twisted ribbons that are assembled from several protofilaments. (*B*) In the presence of Zn^{2+}, the peptide forms clusters of smooth globular shapes. The bar within the insets represents 100 nm.

Like B18, most viral fusion peptides show a strong tendency to self-associate, and an observation of amyloid fibrils has been described in several cases (Wharton et al., 1988; Slepushkin et al., 1993; Pereira et al., 1997; Davies et al., 1998a). Because the formation of amyloid fibrils is critically dependent on peptide sequence rather than just hydrophobicity, it has even been speculated that the amyloidogenic nature might be a common and relevant feature of fusion peptides (Gordon et al., 1992).

Transition metal ions bind to the histidine-rich motif of B18, and this also causes the peptide to precipitate, although

in a manner different from that of B18 per se. Negative stain EM shows that the peptide-Zn^{2+} complexes form smooth globular clusters (Fig. 1 *B*), consisting of small bulges with a diameter typically between 50 and 70 nm. A similar appearance is observed for B18 in the presence of Cu^{2+} (data not shown). It is known that Zn^{2+} triggers the fusogenic activity of the peptide, whereas Cu^{2+} has an inhibitory effect (Ulrich at al., 1998). According to circular dichroism, the peptide becomes partially α-helical in the Zn^{2+} complex, whereas Cu^{2+} induces a β-turn conformation in the histidine-rich motif (Ulrich at al., 1998). The different conformational characteristics of B18 in the presence of Zn^{2+} and Cu^{2+} cannot be discriminated on behalf of the morphological pictures obtained by EM. Nevertheless, it is clear that the binding of metal ions to the histidine-rich motif of the peptide induces a kind of self-association that is distinctly different from the fibrillar amyloid structure formed by B18 per se.

Structural characterization of the B18 fibrils by x-ray and freeze-fracture EM

A characteristic feature of all amyloid fibrils is the regular cross-β-sheet assembly of the peptides or proteins, with a repeat distance of 0.47 nm due to the backbone spacing (Malinchik et al., 1998). Hence, x-ray diffraction was used to check whether the B18 peptide fibrils possess a β-sheet conformation, both in the absence and in the presence of a lipid bilayer. At the same time, the x-ray data provide morphological information about the bilayer dimensions and about the changes induced by the peptide. When the peptide per se is dispersed in aqueous buffer at pH 7.5, it produces the expected x-ray diffraction peak at 2.13 nm^{-1} (Fig. 2 *A*) that is characteristic of amyloid. The same diffraction signal is also detected when B18 is reconstituted with DMPC liposomes (Fig. 2 *B*) or with SM/Chol (data not shown) by cosolubilization at a lipid/peptide ratio of 10:1. Evidently, the peptide forms amyloid fibrils not only in buffer but also in the presence of lipids. The characteristic peak position in the diffractograms does not change between −40°C and 50°C, indicating that the β-sheet assembly is stable over this temperature range and that it remains unaffected by the DMPC phase transitions (data not shown).

The x-ray diffractograms of Fig. 2 were acquired over both the small-angle and wide-angle diffraction regions, to examine not only the lamellar spacing (small angle), but also the lateral lipid packing (wide angle) of the bilayers. The diffraction peaks in the small-angle region are broad-

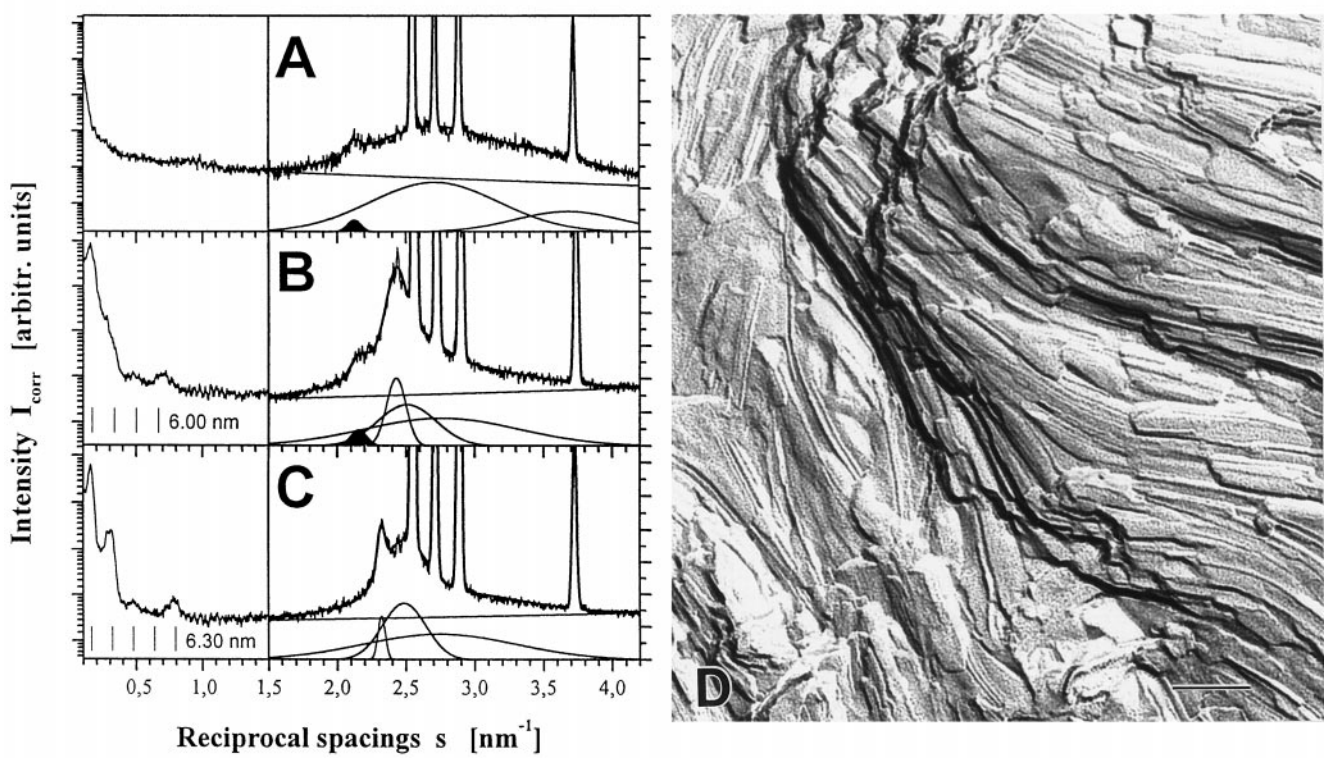

FIGURE 2 Combined small-angle and wide-angle x-ray diffractograms of (*A*) the peptide in aqueous buffer, (*B*) B18 reconstituted with DMPC (lipid/peptide ratio of 10:1), and (*C*) multilamellar DMPC liposomes at −10°C. Deconvolution of the wide angle diffraction regions reveals a characteristic β-sheet spacing of 0.47 nm for the peptide (*shaded peaks*), which proves that it forms amyloid fibrils both in buffer (*A*) and in the presence of the lipid (*B*). The bilayer repeat distance is slightly decreased in the presence of B18, as indicated by the arrays of lines in the small-angle regions of *B* and *C*. The deformed hexagonal lipid packing in the gel state is also affected, as seen by the positions and widths of the deconvoluted peaks in the wide-angle regions of *B* and *C*. The lipid/peptide sample used for *B* was also characterized by EM (*D*), revealing a high density of parallel structures that are attributed to peptide fibrils. The shadowing direction of this and all further EM images is oriented from bottom to top, and the bar represents 100 nm.

ened by the presence of B18, indicating that the peptide reduces the long-range order of stacked bilayers in the sample. Quantitative analysis shows that the bilayer repeat spacing decreases slightly from 6.3 nm (Fig. 2 *C*) to 6.0 nm (Fig. 2 *B*), which could be due to a change in lipid hydration upon peptide binding. The data shown in Fig. 2 were selected at a temperature of −10°C, where DMPC is in the gel phase, because here the wide-angle region carries further information about the lipid packing in the plane of the membrane. The diffractograms in Fig. 2 have been deconvoluted into sets of curves, whose positions and widths represent the deformed hexagonal array of the lipid acyl chains. A qualitative comparison of these respective curves shows that the in-plane acyl chain packing of pure DMPC (Fig. 2 *C*) is significantly affected by the peptide (Fig. 2 *B*). The perturbations of the acyl chain packing together with the changes in bilayer dimensions therefore suggest that the lipid molecules are in direct contact with the amyloid fibrils. This conclusion is further supported by the fact that the phase transition of DMPC is significantly broadened in the presence of B18, as observed by an x-ray temperature scan (data not shown). Differential scanning calorimetry confirms that the pretransition of DMPC disappears and that the main peak is progressively broadened and reduced to a small hump by increasing amounts of peptide (data not shown). An analogous series of x-ray experiments with B18 in SM/Chol gave essentially the same kind of picture as shown in Fig. 2 for DMPC. The only difference is that the acyl chain packing of natural SM is less ordered in the gel phase, because of its composition of saturated and unsaturated acyl chains; hence the SM/Chol data were not picked for illustration purposes. We also note that there were no diffraction peaks indicative of an H_{II} lipid structure, and no hexagonal or cubic phases were detected by ^{31}P-NMR (Grage et al., manuscript in preparation).

The x-ray samples were characterized further by freeze-fracture EM at room temperature. The image of the DMPC sample reconstituted with B18 (Fig. 2 *D*) shows many parallel ridges, along which the monolayers seem to fracture with particular ease. Such morphology may appear vaguely reminiscent of bilayer ripples or inverted hexagonal phases. However, they must be due to peptidic structures, in view of the fibrils observed by negative stain EM (Fig. 1 *A*) and by x-ray diffraction (Fig. 2). Together with our ^{31}P-NMR observations (Grage et al., manuscript in preparation), these data rule out the formation of hexagonal lipid phases. To be sure that any kind of rippled lipid morphology can also be excluded, B18 was reconstituted with several other types of lipid for comparison. The samples shown in Fig. 3 consist of a higher lipid/peptide ratio (30:1), so that there is a greater area in which to observe lipidic structures. Like DMPC, DMPG is known to form characteristic asymmetrical ripples, which are seen in the reconstituted bilayer with a periodicity of ~15 nm (Fig. 3 *A*). Furthermore, distinct peptide fibrils can be discerned in the same image, which are preferentially aligned parallel to the intrinsic lipid ripples. Therefore, it appears that the negative charge of

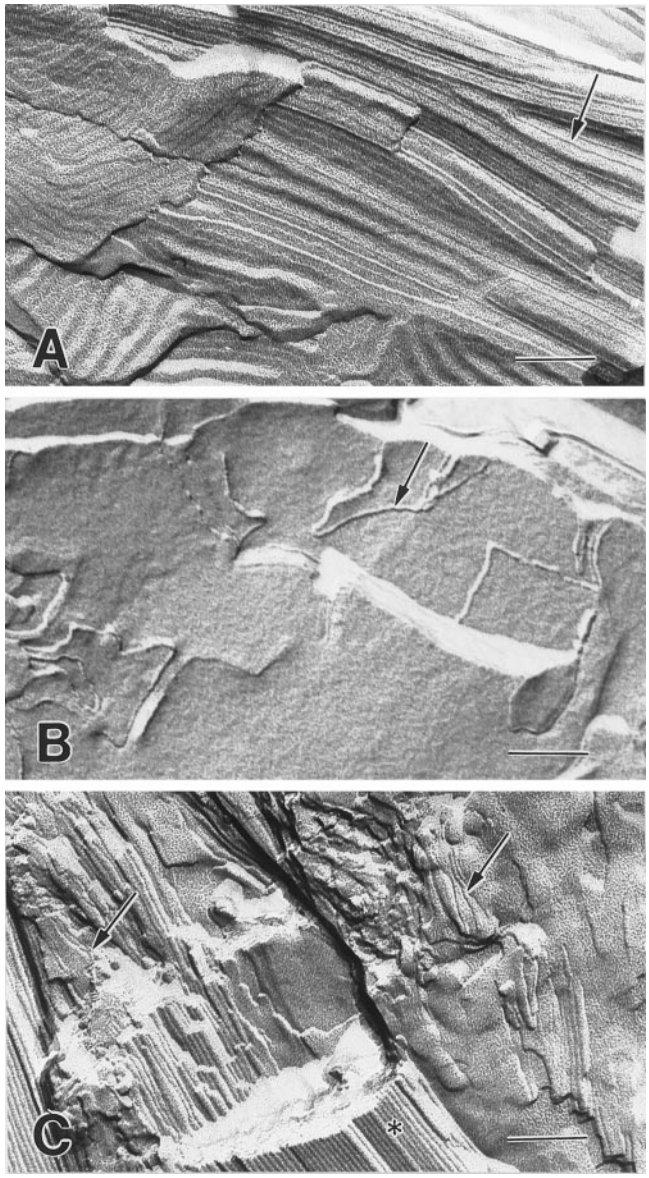

FIGURE 3 Reconstituted samples of B18 with different types of lipid, prepared by cosolubilization in organic solvent at a lipid/peptide ratio of 30:1, and observed by freeze-fracture EM at room temperature. (*A*) In the case of DMPG, which has an intrinsic tendency to form ripples, the peptide fibrils (*arrow*) are aligned parallel to the ripples and with the same spacing. (*B*) In the flat bilayer of egg-PC the peptide fibrils (*arrow*) are more crooked. (*C*) DOPE forms H_{II} phase tubuli (*asterisk*), which do not support a parallel arrangement of the fibrils that are visible in other areas of the image (*arrows*). The bar represents 100 nm.

DMPG does not influence the binding mode of the positively charged peptide fibrils, compared to zwitterionic DMPC. In egg-PC, which has no tendency to form ripples, several fibrillar structures are visible in the bilayer (Fig. 3 *B*). Here the peptide fibrils are more irregular and crooked, which is consistent with the lack of a preferred direction that would otherwise be dictated by some intrinsic lipid ripples. Finally, the reconstituted DOPE sample shows not only the characteristic inverted H_{II} cylinders expected for this lipid (*asterisk* in Fig. 3 *C*); it also contains regions where B18

fibrils coexist with the lipid. All of these observations argue that the fibrillar structures on the fracture faces of the lipids must indeed represent amyloid fibrils formed by B18 in a β-sheet conformation, rather than lipidic structures. The fibrillar width observed in these freeze-fracture images is compatible with the ~5-nm diameter of the single protofilaments described above by negative stain EM.

Similar to our observations with B18, the fusion peptides of HIV gp41, influenza hemagglutinin, and the fertilization protein PH-30 can also bind to membranes in a predominantly β-sheet conformation under certain conditions. Usually this structure correlates with inactivation of their fusogenic activity (Takahashi, 1990; Rafalski et al., 1990; Martin et al., 1993; Gray et al., 1996; Kliger et al., 1997), but in a few cases the β-sheet conformation was reported to possess the highest activity (Nieva et al., 1994; Muga et al., 1994; Pereira et al., 1997; Niidome et al., 1997). Regardless of whether the formation of fibrils by fusion peptides has a general functional relevance or whether they are merely an inactivated by-product, the interaction of amyloid fibrils with lipid bilayers deserves further attention. A diverse range of other proteins is known to form amyloid, sometimes with pathological consequences, as in the case of Alzheimer's and prion-related diseases (Forloni et al., 1996; Kelly, 1997; Malinchik et al., 1998). It has been suggested that the lipid membrane might play a catalytic role in the nucleation or self-assembly process of these fibrils (McLaurin and Chakrabartty, 1996). For example, the surface of negatively charged bilayers is known to promote the β-sheet conformation of the Alzheimer Aβ peptide, presumably as a result of its local accumulation due to electrostatic attraction (Terzi et al., 1997; McLaurin et al., 1998). Our study of B18 supports the notion that the membrane may serve as a steric or dielectric template in the deposition of fibrils, because the self-association of B18 occurs at lower concentration in the presence of lipid than without. Although the Aβ peptide is supposed to adhere electrostatically to the bilayer surface, the binding of B18 must be dominated by hydrophobic interactions, as it has a high affinity for uncharged as well as charged membranes. With regard to the pathogenic role of peptide fibrils, it has been speculated that the neurotoxic effects of amyloidogenic peptides might be attributed to a mechanical disruption of the bilayer (Li et al., 1995; McLaurin et al., 1998). In support of this hypothesis, the lateral cohesion of our model bilayers appears to be significantly weakened, as they fracture preferentially along the sites where the peptide fibrils are located (Figs. 3 *B* and 5 *B*).

Fusion of SM/Chol vesicles by B18, as monitored by freeze-fracture EM

The above samples of B18 with DMPC, with SM/Chol, and with other lipids had been reconstituted by cosolubilization in organic solvent, drying, and subsequent hydration. However, this method of sample preparation does not reflect the situation the peptide encounters during its biologically relevant function, where it binds Zn^{2+} ions and induces vesicle fusion. Therefore we now turn to conditions similar to those of a previous study (Ulrich et al., 1998), where the kinetics of B18-induced vesicle fusion had been monitored using SM/Chol vesicles (pH 7.5, 30°C). The lipid composition of 80/20 SM/Chol was chosen because it is known to be a preferred target of the parent protein bindin, whereas the fusion of liquid crystalline DMPC vesicles by the native protein is much slower (Miraglia, 1993; Ulrich et al., 1998). Here we used freeze-fracture EM to examine the fate of large unilamellar SM/Chol vesicles upon exposure to B18 at a lipid/peptide ratio of 30:1, with and without Zn^{2+}. The control experiment in Fig. 4 *A* shows that the original vesicle preparation contains a uniform distribution of LUVs with ~100-nm diameter. When B18 is added per se, most vesicles become reorganized into extended lamellar sheets (Fig. 4 *B*). The fracture faces of these sheets are covered by long parallel peptide fibrils, evenly spaced with ~15-nm lateral separation. The morphology of these membranes after incubation with B18 in aqueous solution is similar to that of the x-ray samples prepared by cosolubilization in organic solvent (e.g., Fig. 2 *D*). The extensive reorganization of LUVs by B18 observed in Fig. 4 *B* is also in good agreement with an earlier fluorescence study, which showed that peptide binding causes a rapid leakage of contents (Ulrich et al., 1998). On the other hand, no significant lipid mixing had been observed in that study; therefore no merging of the vesicles had been expected to occur here. These inconsistent observations might be explained if the rearrangement of the LUVs into extended multilamellar sheets takes place over a much longer time scale than the fluorescence assay. Alternatively, it is possible that the membrane-bound fibrils prevent a rapid lipid mixing by acting as lateral barriers in the bilayer. In any case, the fragmented appearance of the lipid bilayers in Fig. 4 *B* (as well as in many other images of this kind) suggests that B18 per se is not able to induce genuine vesicle fusion in SM/Chol.

To trigger vesicle fusion, the SM/Chol LUVs are exposed to B18 in the presence of Zn^{2+} (1.6 mM). Under these conditions, Fig. 4 *C* shows that most of the LUVs have merged into large assemblies reminiscent of multilamellar liposomes. Their morphology and size are fully consistent with genuine fusion between a very large number of LUVs. The resulting stacks of bilayers show many cross-fractured open ends (*arrow* in Fig. 4 *C*), which indicated a weakening of the monolayers. When quenchend from 30°C, the fracture faces display an irregular pattern of stripes with an in-plane distance of ~30 nm. Rather than interpreting these ridge-like structures as peptide fibrils, we attribute this morphology to an intrinsic deformation of the lipid bilayer. Such deformations have previously been documented for SM/Chol mixtures (Meyer et al., 1998) and for DMPC/Chol (Copeland and McConnell, 1980). In these earlier studies, stripes and ripples were reported for molar ratios of up to 20% Chol, which corresponds to the composition of our bilayer. Because the occurrence of stripes is known to be

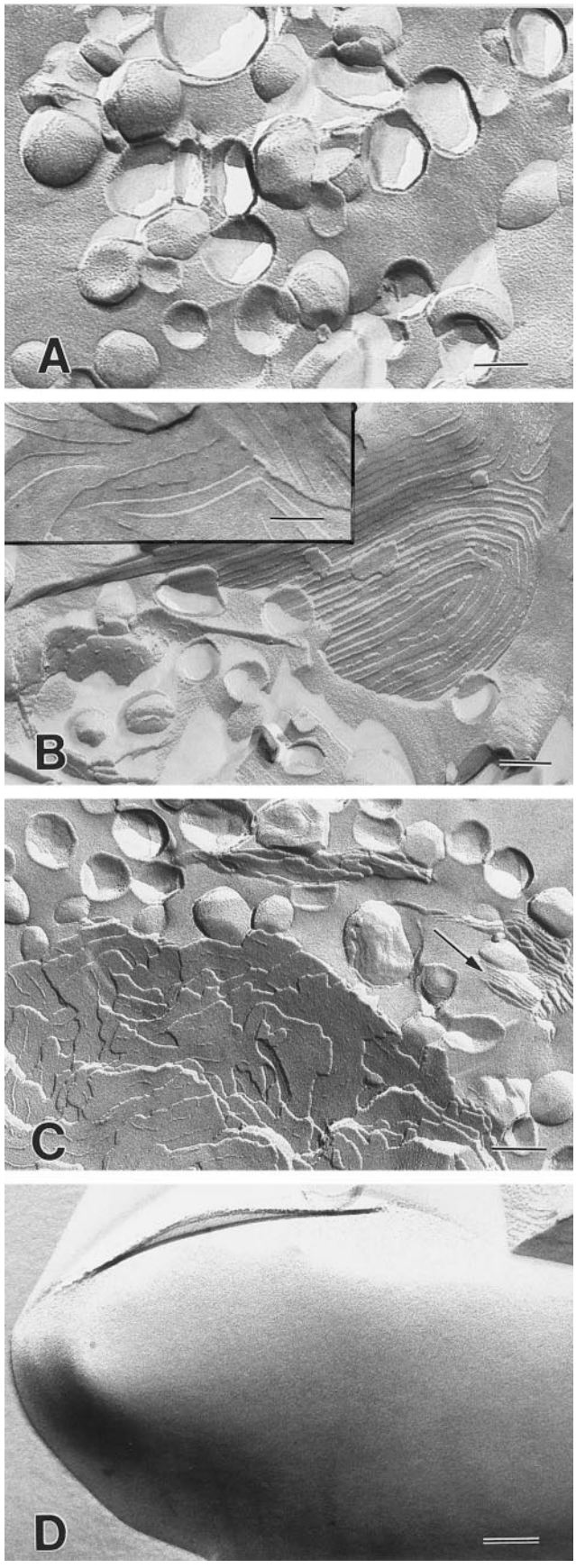

FIGURE 4 Interaction of B18 with SM/Chol (80/20) vesicles in buffer at a lipid/peptide ratio of 30:1, quenched from 30°C and visualized by freeze-fracture EM. (*A*) The original LUVs have a diameter of ~100 nm. (*B*) When B18 is added per se, most of the vesicles reassemble into extended lamellar stacks of bilayers. The peptide forms long parallel fibrils that often demarcate the fractured edges. (*C*) The combined action of B18 and Zn^{2+} triggers extensive fusion of the LUVs into large multilamellar liposomes, which show many cross-fractured open ends (*arrow* in *C*). When the fused sample is kept at 30°C in the gel phase, the bilayers contain some irregular stripes because of the intrinsic propensity of the SM/Chol mixture to form rippled structures. (*D*) After incubation of the same sample at 45°C in the liquid crystalline phase for 30 min, the stripes disappear and the fracture faces of the fused vesicles are entirely smooth. The peptide fibrils, on the other hand, persist after an incubation at 45°C (*inset* of *B*). The bar represents 100 nm.

strongly affected by temperature and by kinetic effects, we incubated the EM sample in its liquid crystalline phase at 45°C for 30 min. As a result, in Fig. 4 *D* the irregular stripes have disappeared and the fracture faces are entirely smooth. Hence there is no evidence of any lipidic or peptidic patterns in the SM/Chol vesicles after they have been fused by the combined action of B18 and Zn^{2+}. In contrast, the B18 amyloid fibrils in the sample without Zn^{2+} (Fig. 4 *B*) persisted in the bilayer when incubated at high temperature (Fig. 4 *B, inset*). Finally, we also incubated the set of EM samples at 4°C (data not shown), but no significant morphological differences were observed.

Fusion of DMPC vesicles by B18, as monitored by freeze-fracture EM

Electron microscopy has provided evidence for the B18-induced fusion of vesicles composed of SM/Chol in the presence of Zn^{2+}. However, the effect of the bilayer phase state on the lipid-peptide and peptide-peptide interactions could not be clearly discerned in this lipid system, because the phase transition of the SM/Chol mixture is very broad and rather ill-defined around 30–40°C (Meyer et al., 1999). Therefore, we extended the EM study to include DMPC (see also the x-ray analysis above), which has the same phosphocholine headgroup as SM but undergoes a sharp gel-to-liquid-crystalline phase transition at 23°C.

The overview panels in Fig. 5 demonstrate that the B18 peptide is fully capable of inducing fusion of DMPC, unlike the native parent protein that prefers SM/Chol. The images on the right-hand side show important details about the fracture faces at higher magnification. It is seen that most of the original LUVs (Fig. 5 *A*) become reorganized into lamellar bundles when exposed to B18 per se (Fig. 5 *B*). Again, the appearance of the peptide fibrils in DMPC is similar to the data with SM/Chol (Fig. 4 *B*) and the other reconstituted lipid samples (Fig. 2). Furthermore, besides the fibrous bundles of B18 and DMPC in Fig. 5 *B*, a few vesicles with moderately increased sizes are observed in the same picture, which appear to have formed by weak fusion of LUVs. A very extensive fusion, on the other hand, is observed only in the presence of Zn^{2+} (0.6 mM) in Fig. 5 *C*, as expected. We also tested a higher Zn^{2+} concentration

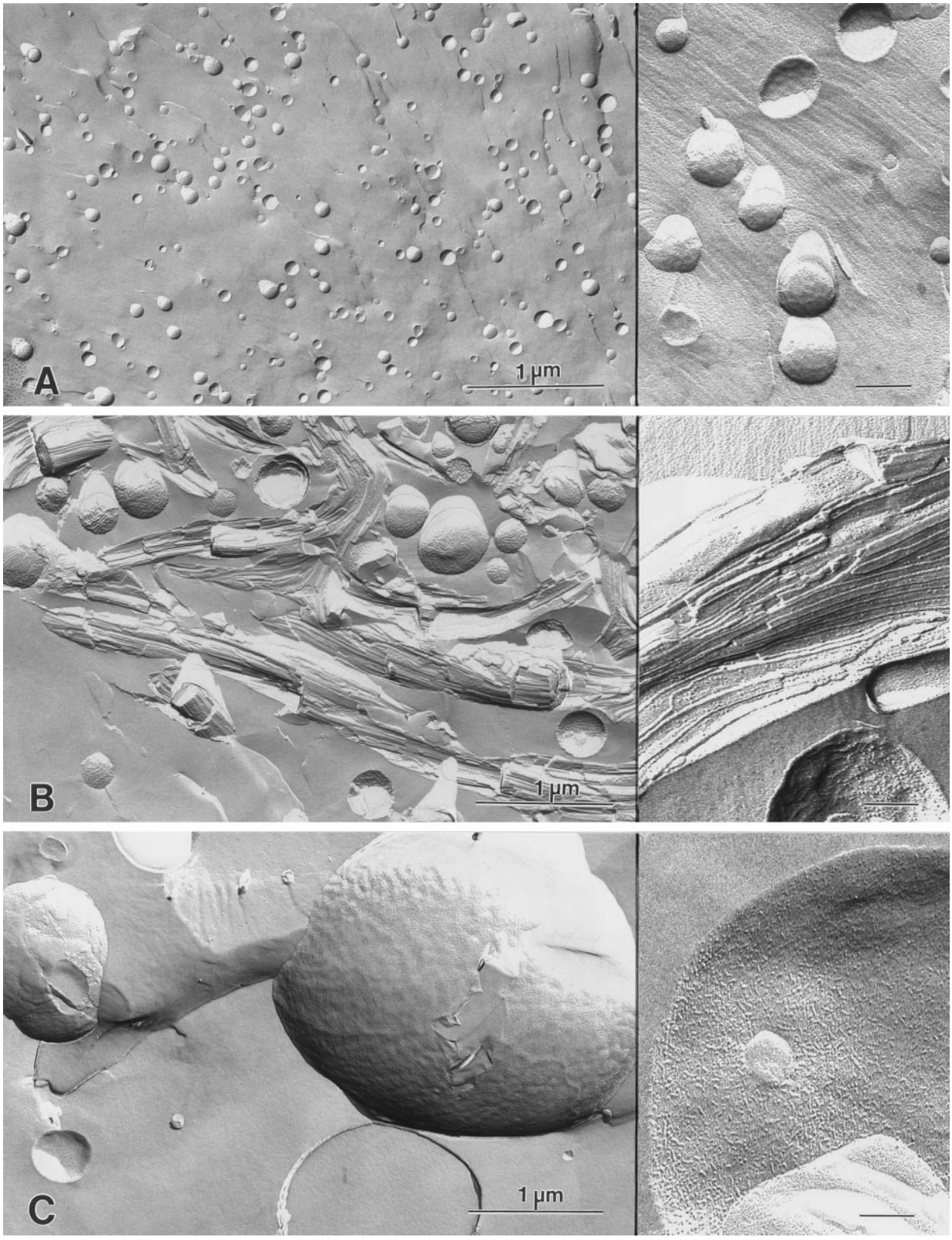

FIGURE 5 Interaction of B18 with liquid crystalline DMPC at a lipid/peptide ratio of 30:1 at 30°C. All overview panels on the left are shown on the same scale, and the insets on the right have a fourfold higher magnification. (*A*) The original LUVs have a diameter of ~100 nm. (*B*) The addition of B18 per se causes the lipid to reorganize into extended lamellar bundles that are closely associated with many parallel peptide fibrils. In addition, a few medium-sized vesicles are formed by fusion, and their fracture faces contain small particles. (*C*) When fusion is triggered by the combined action of B18 and Zn^{2+}, the vesicle size increases dramatically and all fracture faces are densely covered with small particulate structures, which are attributed to peptidic aggregates. The bar within the insets represents 100 nm.

(3.3 mM, data not shown), but fusion was inefficient in this range, which is consistent with a previous report that excess Zn^{2+} prevents fusion, presumably because of rapid peptide precipitation (Ulrich at al., 1998). Interestingly, the fracture faces of the fused vesicles in Fig. 5 *C* contain a high density of small particles. At first sight, their appearance may be vaguely reminiscent of the irregular stripes observed with SM/Chol. However, the stripes in the SM/Chol membranes had disappeared by incubation in the liquid crystalline phase, whereas these particulate structures persist in DMPC. Therefore, these structures cannot be attributed to intrinsic bilayer ripples.

The EM data in Fig. 6 illustrate the response of the DMPC samples to a reduction in temperature, to be compared with Fig. 5, where the lipid was in the liquid crystalline L_α phase at 30°C. When incubated at 4°C and 18°C, the bilayers form a tilted gel phase $L_{\beta'}$ and a ripple phase $P_{\beta'}$, respectively. The EM picture in Fig. 6 *A* confirms that the pure lipid vesicles are in the gel state at 4°C, because the bilayer prefers to flatten out locally like a honeycomb. At 18°C the LUVs become rippled, with a characteristic periodicity of ~20 nm (Fig. 6 *B*). When exposed to B18 per se, the fracture faces of the lipids contain the expected peptide fibrils at 4°C (Fig. 6 *C*). At 18°C, the fibrils become aligned with the intrinsic lipid ripples (Fig. 6 *D*), as had been observed with DMPG in Fig. 3 *A*. When the DMPC vesicles are fused by the combined action of B18 and Zn^{2+} and incubated at 4°C, small particles are seen in the bilayer plane (Fig. 6 *E*). Compared to the data at 30°C (Fig. 5 *C*), however, a further phase segregation is evident here. At 4°C the particulate structures are excluded from the lipid domains and form a honeycomb network ~30 nm in diameter, which allows the gel phase bilayers to flatten out locally. At 18°C, this network disintegrates into irregular strings of small particles (Fig. 6 *F*), the presence of which suppresses the formation of lipid ripples (cf. Fig. 6, *B* and *D*). Because ripples are known to respond in a sensitive manner to any additives in the bilayer, this observation is consistent with a binding and a partial immersion of B18 in the membrane, not only in its fibrillar state (as concluded above), but also in the presence of Zn^{2+}.

Self-association of peptidic particles in the membrane

What is the nature of the small particles on the fracture faces of the large DMPC vesicles that became fused by the combined action of B18 and Zn^{2+}? The particles seen in Fig. 5 *C* (and on all other images of that kind) occur at a high density, they have a diameter of ~5 nm, and they do not disappear upon incubation in the liquid crystalline phase. To draw further conclusions about the mechanism of B18-induced fusion, it must be clarified whether they represent peptidic structures, like the amyloid fibrils, or whether they have a lipidic origin, such as inverted micelles. In previous freeze-fracture studies of amphiphilic peptides, similar bulges and pits have often been interpreted in terms of lipidic structures such as inverted micelles (Verkleij et al., 1984; Burger, 1998). Indeed, ^{31}P-NMR and x-ray diffraction studies have shown that various peptides are able to induce hexagonal, isotropic, or cubic phases in certain lipids, and this ability appears to correlate with their fusogenic activity (Epand et al., 1992; Colotto and Epand, 1997; Davies et al., 1998a; Yeagle, 1998). It has also been well documented that many compounds with a tendency to form nonbilayer structures promote fusion by facilitating the local monolayer curvature of the transition states (Chernomordik et al., 1995; Bailey and Cullis, 1998).

In the case of B18, however, we do not attribute the membrane-embedded particles to any nonbilayer lipid phases. That is, DMPC has no intrinsic tendency to form inverted structures in view of its bulky headgroup. Even when stimulated by gramicidin A, for instance, only ~30% of H_{II} phase was observed in DOPC at a lipid/peptide ratio of 10:1 (Tournois et al., 1990). It is unlikely that B18 could induce such a high abundance of inverted micelles in Fig. 5 *C* at the comparatively high lipid/peptide ratio of 30:1. Furthermore, our ^{31}P-NMR studies showed essentially no isotropic component (Grage et al., manuscript in preparation). Therefore, we conclude that the small particles represent peptidic clusters of B18 in the membrane, just as the fibrillar structures represent amyloid rather than a lipidic H_{II} phase. To be visible by EM, the small particles must consist of ~50 peptides or more, and their size may be limited by the bilayer thickness. These small particles may even be regarded as analogous to the larger clusters formed by B18 and Zn^{2+} in aqueous buffer (Fig. 1 *B*), thus emphasizing the tendency of B18 to self-associate as a metallocomplex. It is nevertheless important to recall at this point that the fused SM/Chol vesicles contain no visible peptidic particles (Fig. 4 *C*). This behavior suggests that the B18-metallocomplexes are better soluble in the more heterogeneous environment of the natural SM, which has a mixed acyl chain composition (Meyer et al., 1999).

Inspection of the distribution of the small particles in DMPC allows further conclusions about the mechanism of fusion. At first sight it appears that the fusogenic activity of B18 is simply triggered by the binding of Zn^{2+}, and that the resulting metallocomplexes can then self-associate further in the DMPC bilayer. However, the medium-size DMPC vesicles in Fig. 5 *C* that are formed in the presence of B18 per se, notably without any Zn^{2+}, also show an abundance of small peptidic particles on their fracture faces (*inset* of Fig. 5 *B*). In contrast, the fibrillar bundles in the same image contain hardly any of these particles interspersed between the peptide fibrils. These observations are functionally significant, as they suggest that the occurrence of the small particles in DMPC is intimately related to membrane fusion, rather than being due to the presence of Zn^{2+}. Hence the binding of Zn^{2+} is not an essential requirement for fusion activity or for the formation of small particles in the membrane. Instead it appears that, even without Zn^{2+}, a small fraction of the peptide population can fold directly into an

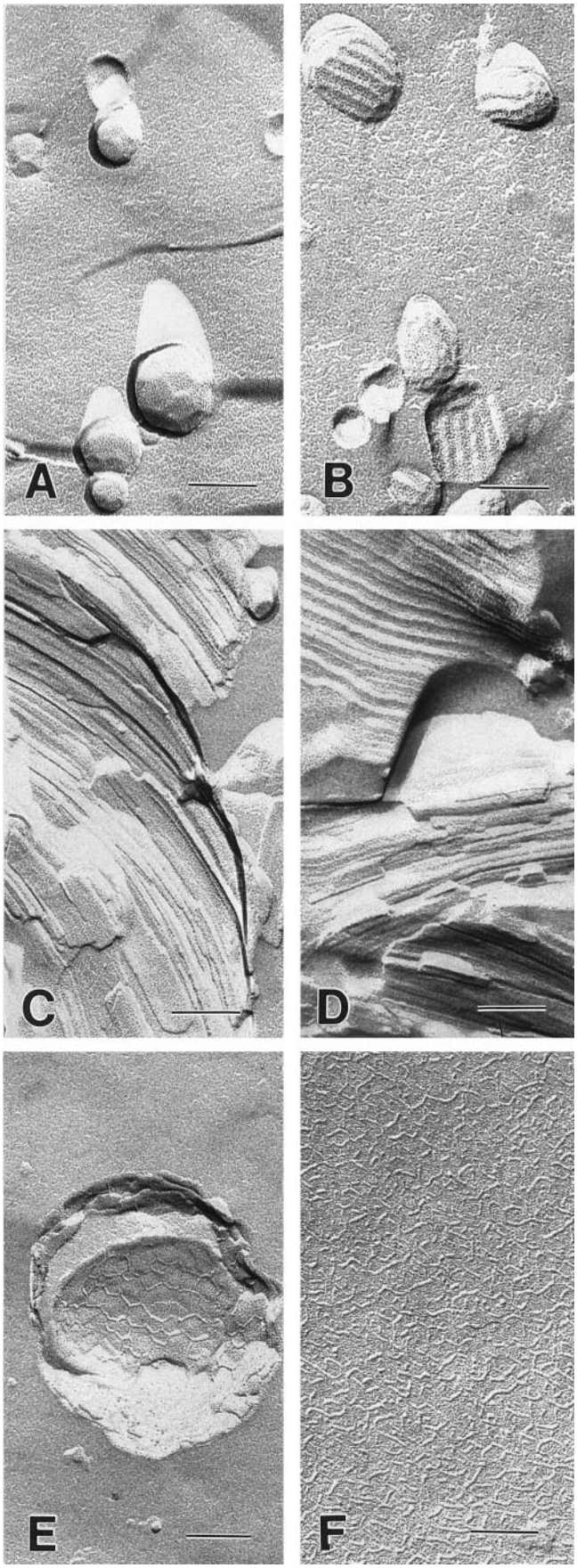

active conformation and lead to a moderate fusion of DMPC. The binding of Zn^{2+} must therefore play an indirect role, presumably by shifting an intrinsic conformational equilibrium of B18 all the way into its fusogenic structure, and by preventing the deposition of inactivated amyloid fibrils.

Another question in the interpretation of B18-lipid interactions concerns the localization of the fibrillar and particulate structures in the bilayer. Whereas freeze-fracture EM reveals the hydrophobic membrane interior, the hydrophilic bilayer surface can be uncovered by freeze-etching (Tillack and Marchesi, 1970; Pinto-da-Silva and Branton, 1970). By using a combination of these techniques, the position of a membrane-bound object can be qualitatively attributed either to the bilayer surface or to its interior. The freeze-etched images of Fig. 7 show DMPC vesicles that have been exposed to B18 per se (Fig. 7 *A*) and to B18 plus Zn^{2+} (Fig. 7 *B*). Close inspection of these data (and of many other representative examples) shows that the hydrophilic bilayer surfaces are relatively smooth compared to the hydrophobic fracture faces. Therefore, we conclude that both the peptide fibrils and the particulate structures are accommodated largely within the hydrophobic bilayer core. The same result is obtained with SM/Chol, where the fibrillar structures are observed by freeze-etching EM to be more sharply defined in the bilayer interior. These observations add weight to our interpretation that the peptide must interact directly with the lipid chains, both in its inactivated fibrillar and in its functional state.

CONCLUSIONS

The aim of this study was to obtain better insight into the lipid-peptide and peptide-peptide interactions related to membrane fusion, and to draw conclusions about any relevant structural requirements. A fusogenic activity for the B18 sequence of the sea urchin sperm protein bindin had recently been proposed on the basis of conventional fluorescence assays (Ulrich et al., 1998). Even though these methods provide a powerful and rapid strategy for monitoring lipid mixing or contents mixing, an exchange of fluorescent markers can also occur during aggregation, hemifusion, or other peptide-induced bilayer rearrangements (Ohki et al., 1998). Therefore, to be certain that genuine fusion has taken place, it is advisable to monitor the resulting vesicle sizes and shapes by electron microscopy (Kliger et al.,

FIGURE 6 Effect of temperature on the interaction of DMPC vesicles (*top row*) with B18 per se (*middle row*), and with B18 plus Zn^{2+} (*bottom row*). (*A*) When incubated and quenched from 4°C (*left-hand column*), the pure lipid forms the flat $L_{\beta'}$ phase. (*B*) At 18°C (*right-hand column*) it forms the rippled $P_{\beta'}$ phase. (*C*) When B18 is added per se, peptide fibrils are seen on the bilayer fracture faces at 4°C. (*D*) The fibrils align with the intrinsic lipid ripples at 18°C. (*E*) In the presence of both B18 and Zn^{2+}, small peptidic particles are seen to be segregated from the lipid at 4°C into a higher-order honeycomb network. (*F*) This network breaks up at 18°C and suppresses the formation of lipid ripples. The bar represents 100 nm.

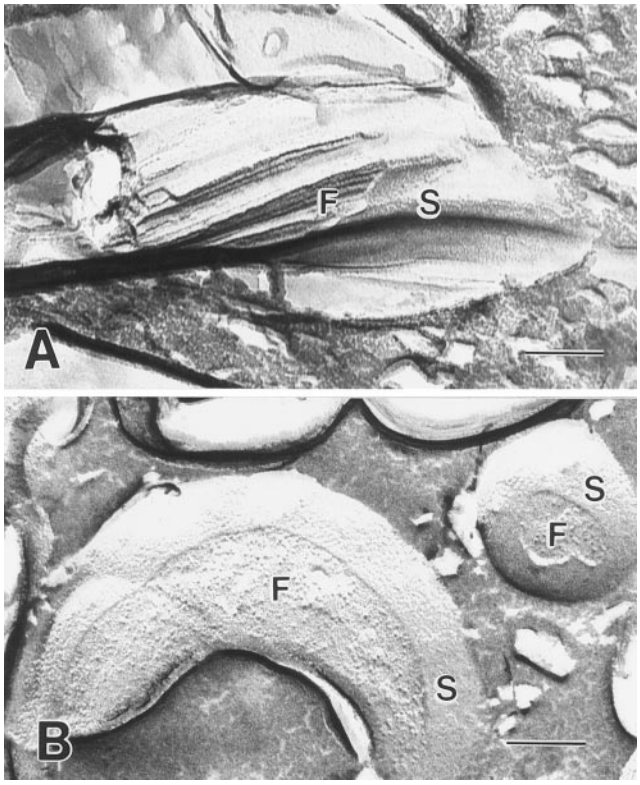

FIGURE 7 Localization of the fibrillar and particulate structures of B18 in DMPC at 30°C, as revealed by freeze-etching EM. (*A*) The fibrils composed of B18 per se appear to be located in the bilayer interior, because the etched membrane surface (S) is much smoother than the fractured hydrophobic face (F). (*B*) The small particulate structures formed in the presence of B18 plus Zn^{2+} also seem to reside mainly within the bilayer core. The bar represents 100 nm.

1997; Rapaport and Shai, 1994). Here it has been confirmed by EM that the B18 peptide can induce extensive vesicle fusion when triggered by Zn^{2+}, which underscores the relevance of these lipid-protein interactions during fertilization.

Concerning the model character of the B18 system, it is remarkable that the amphiphilic peptide leads to extensive fusion between uncharged SM/Chol as well as DMPC vesicles. The parent protein bindin adheres only to lipid bilayers in the gel phase, and it fuses SM/Chol much faster than DMPC (Miraglia, 1993; Loidl-Stahlhofen et al., 1996), which may reflect the specific lipid composition of the acrosomal membrane (Hofmann and Glabe, 1994; Vacquier et al., 1995). In the case of B18, however, our data suggest that nonspecific hydrophobic interactions are sufficient for anchoring the peptide to any kind of lipid bilayer. Having demonstrated the fusogenic character of B18 and several conformational similarities with viral fusion peptides, it is likely that this peptide sequence is indeed responsible for the fusogenic function of bindin, by inserting into and destabilizing the membrane of either sperm or egg (Hughson, 1995; Hernandez et al., 1996; Monck and Fernandez, 1996; Pécheur et al., 1999). Besides these biological implications, the B18 model has made it possible to address some fundamental aspects of peptide-induced fusion processes in a system whose structure is conveniently regulated by the presence of Zn^{2+} ions (Shai, 1995; Brasseur et al., 1997).

It has been demonstrated here that the B18 peptide can self-assemble into two different kinds of supramolecular structures, namely as fibrils or as globular particles. These two forms have different conformations, and they represent different functional states of B18. The peptide per se forms fibrils at pH $>$ 7, both in aqueous buffer as well as in lipid membranes composed of SM/Chol, DMPC, DMPG, egg-PC, or DOPE. The fibrils possess a β-sheet structure that is characteristic of amyloid, as confirmed by x-ray diffraction and Congo Red staining. The peptide is not fusogenic in the β-sheet conformation, although the fibrils interact strongly with the lipid bilayer and render the membrane fragile. This observation might bear some relevance to the neurotoxic effects of amyloidogenic peptides that may cause Alzheimer's and prion-related diseases by disrupting cellular membranes.

A distinctly different mode of B18 self-assembly takes place in the presence of Zn^{2+}, which is used to trigger the fusogenic activity of the peptide. The biological role of Zn^{2+} is supported by the fact that native sperm bindin contains a stoichiometric amount of this specific metal ion, bound to the histidine-rich motif of the B18 sequence (DeAngelis and Glabe, 1990b). In aqueous buffer containing Zn^{2+}, we found that the peptide self-assembles into smooth globular clusters of about 50-nm diameter. According to a previous CD study, the secondary structure of B18 is partially α-helical under these conditions (Ulrich et al., 1998). Specific histidine residues in the B18 sequence (H109 and H113) stabilize the local conformation in the Zn^{2+} complex, as their spacing is characteristic of a helical metal binding site (Regan, 1995; Magdaleno et al., manuscript in preparation). A recent NMR study of B18 in either 30% TFE or in detergent micelles has demonstrated that the peptide also assumes a predominantly α-helical conformation in such membrane-mimetic environments (Glaser et al., 1999). Interestingly, at low concentrations (around 15%) of TFE, B18 was observed to form aggregates that look very similar to those in the presence of Zn^{2+} and have a helical secondary structure. The fact that the self-assembly of B18 in an α-helical conformation is possible without Zn^{2+} demonstrates that direct Zn^{2+} bridges are not necessary to make intermolecular contacts, as had been speculated earlier. Instead, we conclude now that self-association occurs when B18 exposes a helical hydrophobic surface to its neighbours. The role of Zn^{2+} is to promote this helical peptide conformation, thereby preventing its aggregation as β-sheet fibrils.

Electron microscopy provides further details about the aggregation behavior of the B18 peptide under fusogenic conditions, by the observation of different kinds of lipid vesicles after fusion in the presence of Zn^{2+}. In the case of SM/Chol, no peptidic structures are observed by EM, which indicates that the B18-metallocomplexes are evenly distributed in the membrane. From the EM data alone, however, it is not possible to assess whether any low-number oligomers

are formed. In the DMPC bilayer, on the other hand, visible peptidic particles (~5 nm) are found after fusion, corresponding to clusters of ~50 monomers. The reduced solubility of B18 in DMPC may be attributed to the uniform acyl chain composition, or to some other kind of hydrophobic mismatch. The comparison of SM/Chol with DMPC has thus illustrated that the self-assembly of the peptide into visible clusters depends subtlely on the lipid environment. Because the peptidic particles in DMPC are a clear indication that fusion has taken place, our data show that some local fusion events can be induced by B18 per se, even in the absence of Zn^{2+}. Therefore, membrane fusion correlates with this particular mode of peptide self-assembly in the bilayer, rather than with the presence of Zn^{2+}.

In a previous report it was suggested that the mechanism of B18-induced vesicle fusion could proceed via a "*trans*" complex, where the Zn^{2+} ion forms an intermolecular bridge between the histidine side chains of two apposing membrane-bound peptides (Ulrich et al., 1998). In view of the details discussed here, we are now able to refine the picture of the fusogenic peptide complex. Rather than constituting a physical bridge between vesicle-bound peptides, the role of Zn^{2+} is to impose a local helical conformation on the peptide backbone, thereby preventing its inactivation as β-sheet fibrils. We conclude that the α-helical structure is the critical factor for the fusogenic function of B18, rather than Zn^{2+} binding as such. Any alternative folding pathways leading to β-sheet fibrils (as preferred by B18 per se) or to a local β-turn (promoted by Cu^{2+}; Ulrich et al., 1998) do not support a fusogenic activity.

In summary, the initially disordered B18 peptide (in the stock solution at pH 4) can fold into two distinct conformational states that compete with one another:

β-Sheet fibril	$\leftarrow$ Random coil $\rightarrow$	α-Helical
(pH > 7)	(pH < 7)	(promoted by Zn^{2+})
Inactivated		*Fusogenic*

A similar conformational flexibility between an active α-helical and an inactive β-sheet structure has been reported for many viral fusion peptides (Kliger et al., 1997; Durell et al., 1997; Gray et al., 1996; Rapaport and Shai, 1994; Martin et al., 1993; Gordon et al., 1992; Rafalski et al., 1990; Takahashi, 1990). Even the prototypical amyloidogenic Alzheimer Aβ peptide is able to fold into an α-helical conformation, whereupon it can form channels and induce membrane fusion (Pillot et al., 1996). Infact, when the Aβ peptide (which like B18 contains three histidine residues) forms a complex with Zn^{2+}, the deposition of amyloid fibrils is attenuated, and its neurotoxicity is reduced (Kawahara et al., 1997). This example emphasizes the difference between peptide-induced vesicle fusion and membrane disruption, and these two separate functions appear to involve different secondary structures.

In view of the conformational polymorphism of viral fusion peptides, it has been suggested that they might generally require a high conformational flexibility to interact with the membrane (Davies et al., 1998b). Indeed, it is well known that the preferred structure of many membrane-binding peptides depends critically on the particular experimental conditions, such as lipid type, pH, or solvent history. Hence it is not uncommon that different studies on a certain peptide report varying degrees of α-helical and β-sheet conformations, which might be an indication that active and inactivated populations coexist. The convenient aspect of the B18 peptide is that its conformation, and hence its fusogenic activity, can be largely controlled by the binding of Zn^{2+}, which acts as a local folding device.

We are grateful to Richard Jacob (EMBL Heidelberg) for synthesizing the peptide. We also thank C. Kämnitz, I. Herrmann, and R. Kaiser for technical assistance in the laboratory, and G. Engelhardt and G. Vöckler for their help with the photographs.

All authors acknowledge the Deutsche Forschungsgemeinschaft for supporting the projects A1, A10, A17, B1, and B13, in the SFB 197.

REFERENCES

Bailey, A. L., and P. R. Cullis. 1998. Liposome fusion. *In* Current Topics in Membranes, Vol. 44. R. M. Epand, editor. Academic Press, San Diego. 359–373.

Brasseur, R., T. Pillot, L. Lins, J. Vanderkerckhove, and M. Rosseneu. 1997. Peptides in membranes: tipping the balance of membrane stability. *Trends Biochem. Sci.* 22:169–171.

Burger, K. N. J. 1998. Morphology of membrane fusion. *In* Current Topics in Membranes, Vol. 44. R. M. Epand, editor. Academic Press, San Diego. 403–445.

Chernomordik, L. V., M. M. Kozlov, and J. Zimmerberg. 1995. Lipids in membrane fusion. *J. Membr. Biol.* 146:1–14.

Colotto, A., and R. M. Epand. 1997. Structural study of the relationship between the rate of membrane fusion and the ability of the fusion peptide of influenza virus to perturb bilayers. *Biochemistry.* 36:7644–7651.

Davies, S. M. A., R. F. Epand, J. P. Bradshaw, and R. M. Epand. 1998a. Modulation of lipid polymorphism by the feline leukemia virus fusion peptide: implications for the fusion mechanism. *Biochemistry.* 37: 5720–5729.

Davies, S. M. A., S. M. Kelly, N. C. Price, and J. P. Bradshaw. 1998b. Structural plasticity of the feline leukemia virus fusion peptide: a circular dichroism study. *FEBS Lett.* 425:415–418.

DeAngelis, P. L., and C. G. Glabe. 1990a. Specific recognition of sulfate esters by bindin, a sperm adhesion protein from sea urchins. *Biochim. Biophys. Acta.* 1037:100–105.

DeAngelis, P. L., and C. G. Glabe. 1990b. Zinc specifically stimulates the selective binding of a peptide analogue of bindin to sulfated fucans. *Pept. Res.* 3:1–7.

Durell, S. R., I. Martin, J.-M. Ruysschaert, Y. Shai, and R. Blumenthal 1997. What studies of fusion peptides tell us about viral envelope glycoprotein-mediated membrane fusion. *Mol. Membr. Biol.* 14:97–112.

Epand, R. M., J. J. Cheetham, R. F. Epand, P. L. Yeagle, C. D. Richardson, A. Rockwell, and W. F. DeGrado. 1992. Peptide models for the membrane destabilization actions of viral fusion proteins. *Biopolymers.* 32: 309–314.

Forloni, G., F. Tagliavini, O. Bugiani, and M. Salmona. 1996. Amyloid in Alzheimer's disease and prion-related encephalopathies: studies with synthetic peptides. *Prog. Neurobiol.* 49:287–315.

Glabe, C. G. 1985a. Interaction of the sperm adhesive protein, bindin, with phospholipid vesicles. I. *J. Cell. Biol.* 100:794–799.

Glabe, C. G. 1985b. Interaction of the sperm adhesive protein, bindin, with phospholipid vesicles. II. *J. Cell. Biol.* 100:800–806.

Glaser, R., M. Grüne, C. Wandelt, and A. S. Ulrich. 1999. NMR and CD structural analysis of the fusogenic peptide sequence B18 from the fertilization protein bindin. *Biochemistry.* 38:2560–2569.

Gordon, L. M., C. C. Curtain, Y. C. Zhong, A. Kirkpatrick, P. W. Mobley, and A. J. Waring. 1992. The amino-terminal peptide of HIV-1 glycoprotein 41 interacts with human erythrocyte membranes: peptide conformation, orientation, and aggregation. *Biochim. Biophys. Acta.* 1139:257–274.

Gray, C., S. A. Tatulian, S. A. Wharton, and L. K. Tamm. 1996. Effect of N-terminal glycine on the secondary structure, orientation, and interaction of the influenza hemagglutinin fusion peptide with lipid bilayers. *Biophys. J.* 70:2275–2286.

Hernandez, L. D., L. R. Hoffmann, T. G. Wolfsberg, and J. M. White. 1996. Virus-cell and cell-cell fusion. *Annu. Rev. Cell Dev. Biol.* 12: 627–661.

Hofmann, A., and C. G. Glabe. 1994. Bindin, a multifunctional sperm ligand and the evolution of new species. *Semin. Dev. Biol.* 5:233–242.

Hughson, F. M. 1995. Molecular mechanisms of protein-mediated membrane fusion. *Curr. Opin. Struct. Biol.* 5:507–513.

Kawahara, M., N. Arispe, Y. Kuroda, and E. Rojas. 1997. Alzheimer's disease amyloid β-protein forms Zn^{2+}-sensitive, cation-selective channels across excised membrane patches from hypothalamic neurons. *Biophys. J.* 73:67–75.

Kelly, J. W. 1997. Amyloid fibril formation and protein misassembly: a structural quest for insights into amyloid and prion diseases. *Structure.* 5:595–600.

Kliger, Y., A. Aharoni, D. Rapaport, P. Jones, R. Blumenthal, and Y. Shai. 1997. Fusion peptides derived from the HIV type 1 glycoprotein 41 associate within phospholipid membranes and inhibit cell-cell fusion. *J. Biol. Chem.* 272:13496–13505.

Li, W. Y., D. L. Czilly, and L. K. Simmons. 1995. Neuronal membrane conductance activated by amyloid β peptide: importance of peptide conformation. *Brain Res.* 682:207–211.

Loidl-Stahlhofen, A., A. S. Ulrich, S. Kaufmann, and T. M. Bayerl. 1996. Protein binding to supported lecithin bilayers controlled by the lipid phase state: a new concept for highly selective protein purification. *Eur. Biophys. J.* 25:151–153.

Malinchik, S. B., H. Inouye, K. E. Szumowski, and D. Kirschner. 1998. Structural analysis of Alzheimer's β(1–40) amyloid: protofilament assembly of tubular fibrils. *Biophys. J.* 74:537–545.

Martin, I., F. Defrise-Quertain, E. Decroly, M. Vandenbranden, R. Brasseur, and J.-M. Ruysschaert. 1993. Orientation and structure of the N-terminal HIV-1 gp41 peptide in fused and aggregated liposomes. *Biochim. Biophys. Acta.* 1145:124–133.

McLaurin, J., and A. Chakrabartty. 1996. Membrane disruption by Alzheimer β-amyloid peptides mediated through specific binding to either phospholipids or gangliosides. *J. Biol. Chem.* 271:26482–26489.

McLaurin, J., T. Franklin, A. Chakrabartty, and P. E. Fraser. 1998. Phosphatidylinositol and inositol involvement in Alzheimer amyloid-β fibril growth and arrest. *J. Mol. Biol.* 278:183–194.

Meyer, H. W., H. Bunjes, and A. S. Ulrich. 1999. Morphological transitions of brain sphingomyelin are determined by the hydration protocol: ripples re-arrange in-plane and sponge-like networks disintegrate into small vesicles. *Chem. Phys. Lipids.* 99:111–123.

Meyer, H. W., M. Westermann, W. Richter, M. Stumpf, W. Richter, A. S. Ulrich, and C. Hoischen. 1998. Minimal radius of curvature of lipid bilayers in the gel phase state corresponds to the dimension of biomembrane structures "caveolae." *J. Struct. Biol.* 124:77–87.

Minor, J. E., R. J. Britten, and E. H. Davidson. 1993. Species-specific inhibition of fertilization by a peptide derived from the sperm protein bindin. *Mol. Biol. Cell.* 4:375–387.

Miraglia, S. J. 1993. Structure-function analysis of the membrane binding domain of bindin, and the potential role of bindin in plasma membrane fusion. Dissertation. University of California, Irvine.

Miraglia, S. J., and C. G. Glabe. 1993. Characterization of the membrane-associating domain of the sperm adhesive protein bindin. *Biochim. Biophys. Acta.* 1145:191–198.

Monck, J. R., and J. M. Fernandez. 1996. The fusion pore and mechanisms of biological membrane fusion. *Curr. Opin. Cell Biol.* 8:524–533.

Muga, A., W. Neugebauer, T. Hirama, and W. K. Surewicz. 1994. Membrane interaction and conformational properties of the putative fusion peptide of PH-30, a protein active in sperm-egg fusion. *Biochemistry.* 33:4444–4448.

Nieva, J. L., S. Nir, A. Muga, F. M. Goni, and J. Wilschut. 1994. Interaction of the HIV-1 fusion peptide with phospholipid vesicles: structural requirements for fusion and leakage. *Biochemistry.* 33: 3201–3209.

Niidome, T., M. Kimura, T. Chiba, N. Ohmori, H. Mihara, and H. Aoyagi. 1997. Membrane interaction of synthetic peptides related to the putative fusogenic region of PH-30, a protein in sperm-egg fusion. *J. Pept. Res.* 49:563–569.

Ohki, S., T. D. Flanagan, and D. Hoekstra. 1998. Probe transfer with and without membrane fusion in a fluorescence fusion assay. *Biochemistry.* 37:7496–7503.

Pécheur, E. I., J. Sainte-Marie, A. Bienvenue, and D. Hoekstra. 1999. Peptides and membrane fusion: towards an understanding of the molecular mechanism of protein-induced fusion. *J. Membr. Biol.* 167:1–17.

Pereira, F. B., F. M. Goni, A. Muga, and J. L. Nieva. 1997. Permeabilization and fusion of uncharged lipid vesicles induced by the HIV-1 fusion peptide adopting an extended conformation: dose and sequence effects. *Biophys. J.* 73:1977–1986.

Pillot, T., M. Goethals, B. Vanloo, C. Talussot, R. Brasseur, J. Vanderkerckhove, M. Rosseneu, and L. Lins. 1996. Fusogenic properties of the C-terminal domain of the Alzheimer β-amyloid peptide. *J. Biol. Chem.* 46:28757–28765.

Pinto-da-Silva, P., and D. Branton. 1970. Membrane splitting in freeze-etching. *J. Cell. Biol.* 45:598–605.

Rafalski, M., J. D. Lear, and W. F. DeGrado. 1990. Phospholipid interactions of synthetic peptides representing the N-terminus of HIV gp41. *Biochemistry.* 29:7917–7922.

Rafalski, M., A. Rockwell, L. C. van Ginkel, J. D. Lear, W. F. DeGrado, and J. Wilschut. 1991. Membrane fusion activity of the influenza virus hemagglutinin: interaction of HA2 N-terminal peptides with phospholipid vesicles. *Biochemistry.* 30:10211–10220.

Rapaport, D., and Y. Shai. 1994. Interaction of fluorescently labeled analogues of the amino-terminal fusion peptide of Sendai virus with phospholipid membranes. *J. Biol. Chem.* 269:15124–15131.

Regan, L. 1995. Protein design: novel metal binding sites. *Trends Biochem. Sci.* 20:280–285.

Shai, Y. 1995. Molecular recognition between membrane-spanning polypeptides. *Trends Biochem. Sci.* 20:460–464.

Slepushkin, V. A., G. V. Kornilaeva, S. M. Andreev, M. V. Sidorova, A. O. Petrukhina, G. R. Matsevich, S. V. Raduk, V. B. Grigoriev, T. V. Makarova, V. L. Lukashov, and E. V. Karamov. 1993. Inhibition of human immunodeficiency virus type 1 (HIV-1) penetration into target cells by synthetic peptides mimicking the N-terminus of the HIV-1 transmembrane glycoprotein. *Virology.* 194:294–301.

Takahashi, S. 1990. Conformation of membrane fusion-active 20-residue peptides with or without lipid bilayers. Implications of α-helix formation for membrane fusion. *Biochemistry.* 29:6257–6264.

Terzi, E., G. Hölzemann, and J. Seelig. 1997. Interaction of Alzheimer β-amyloid peptide (1–40) with lipid membranes. *Biochemistry.* 36: 14845–14852.

Tillack, W. T., and V. T. Marchesi. 1970. Demonstration of the outer surface of freeze-etched red blood cell membranes. *J. Cell Biol.* 45: 649–653.

Tournois, H., C. H. J. P. Fabrie, K. N. J. Burger, J. mandersloot, P. Hilgers, H. van Delen, J. de Gier, and B. de Kruiff. 1990. Gramicidin A induced fusion of large unilamellar dioleoylphosphatidylcholine vesicles and its relation to the induction of type II nonbilayer structures. *Biochemistry.* 29:8297–8307.

Ulrich, A. S., M. Otter, C. G. Glabe, and D. Hoekstra. 1998. Membrane fusion is induced by a distinct peptide sequence of the sea urchin fertilization protein bindin. *J. Biol. Chem.* 273:16748–16755.

Vacquier, V. D., W. J. Swanson, and M. E. Hellberg. 1995. What have we learned about sea urchin sperm bindin? *Dev. Growth Differ.* 73:1–10.

Verkleij, A. J., J. Leunissen-Bijvelt, B. de Kruijff, M. Hope, and P. R. Cullis. 1984. Non-bilayer phases in membrane fusion. *Ciba Found. Symp.* 103:45–59.

Wharton, S. A., S. R. Martin, R. W. H. Ruigrok, J. J. Skehel, and D. C. Wiley. 1988. Membrane fusion by peptide analogues of influenza virus haemagglutinin. *J. Gen. Virol.* 69:1847–1857.

Yeagle, P. L. 1998. Membrane fusion intermediates. *In* Current Topics in Membranes, Vol. 44. R. M. Epand, editor. Academic Press, San Diego. 375–401.